

Role of bacterial persistence in spatial population expansionPintu Patra^{1,*} and Stefan Klumpp^{2,†}¹*Institute for Theoretical Physics, Heidelberg University, Heidelberg 69120, Germany*²*Institute for the Dynamics of Complex Systems, University of Göttingen, Göttingen 37077, Germany* (Received 16 March 2021; revised 13 August 2021; accepted 19 August 2021; published 2 September 2021)

Bacterial persistence, tolerance to antibiotics via stochastic phenotype switching, provides a survival strategy and a fitness advantage in temporally fluctuating environments. Here we study its possible benefit in spatially varying environments using a Fisher wave approach. We study the spatial expansion of a population with stochastic switching between two phenotypes in spatially homogeneous conditions and in the presence of an antibiotic barrier. Our analytical results show that the expansion speed in growth-supporting conditions depends on the fraction of persister cells at the leading edge of the population wave. The leading edge contains a small fraction of persister cells, keeping the effect on the expansion speed minimal. The fraction of persisters increases gradually in the interior of the wave. This persister pool benefits the population when it is stalled by an antibiotic environment. In that case, the presence of persister enables the population to spread deeper into the antibiotic region and to cross an antibiotic region more rapidly. Further we observe that optimal switching rates maximize the expansion speed of the population in spatially varying environments with alternating regions of growth permitting conditions and antibiotics. Overall, our results show that stochastic switching can promote population expansion in the presence of antibiotic barriers or other stressful environments.

DOI: [10.1103/PhysRevE.104.034401](https://doi.org/10.1103/PhysRevE.104.034401)**I. INTRODUCTION**

Population expansion in space facilitates evolutionary diversification and survival of species [1,2]. Recent experiments using microfluidics have demonstrated the role of spatial structures on population expansion using microbes as model organisms, providing insight into several eco-evolutionary [3–6] and medically relevant questions [7–10]. For example, in spatial environments, cooperative behaviors are sustained [5], positively frequency-dependent selection can persist [11], and the rapid emergence of antibiotic resistance is facilitated [12]. Population survival and competitive strategies are the major driving factors for many of these intriguing behaviors [5,9,13].

A prime example of a population-level survival strategy is bacterial persistence, where the population benefits from a subpopulation with the persister phenotype that is more tolerant to stresses such as antibiotics [14–16]. However, persisters incur a cost due to their slow division rate in growth-supporting conditions [17]. In a temporally changing environment, the interplay between cost and benefit determines the circumstances where persistence is advantageous [18–21]. A population expanding in space could encounter such temporally varying conditions by moving through different environments in space. Therefore, we ask here how bacterial persistence affects the expansion of a population in space and whether a similar cost-benefit trade-off exists in

spatially modulated environments as in temporally varying conditions.

To this end, we study the effect of bacterial persistence in a population spatially expanding in a homogeneous growth-favorable environment and in a scenario where growth is halted by an antibiotic region. We make use of the approach introduced by Fisher [22] and Skellam [23] which has been extensively used to describe the spatial spread of invading species, insects, epidemic agents, and others [24]. This formalism allows us to write a set of wave equations for a population of cells that reversibly switch between the normal growing state and the slow-growing persister state. We determine the cost of persistence during growth conditions by computing the population expansion speed as well as the fitness advantage due to persisters in crossing an antibiotic barrier. The scenarios studied here can be considered idealized descriptions of real environments, for example, in the body of a patient, but more importantly they can directly be realized experimentally with current methods such as spatially structured environments on solid surfaces [7] or in microfluidic devices [8,9,25].

II. MODEL FOR SPATIAL EXPANSION OF A PHENOTYPICALLY HETEROGENEOUS POPULATION

The expansion of populations in space can be described by the Fisher equation (or Kolmogorov-Petrovsky-Piskunov equation)

$$\frac{\partial n}{\partial t} = D \frac{\partial^2 n}{\partial x^2} + \mu[1 - n]n. \quad (1)$$

*Pintu.patra@bioquant.uni-heidelberg.de

†Stefan.klumpp@phys.uni-goettingen.de

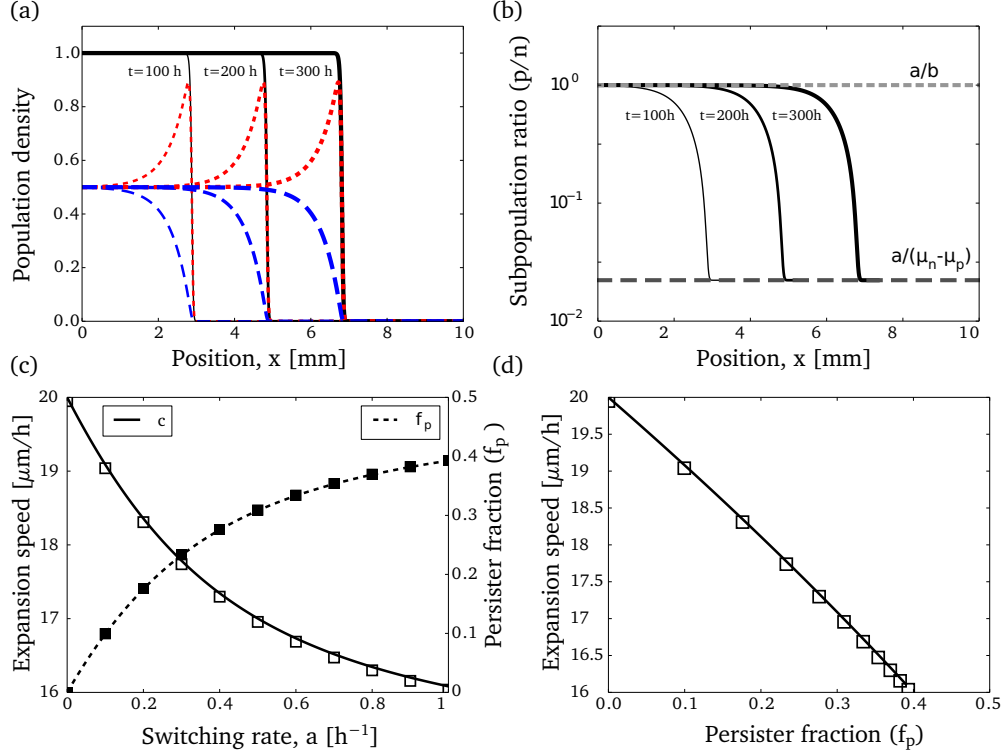


FIG. 1. (a) The model equations display traveling waves moving with a constant expansion speed. The total population density (black line) wave has contributions from two subpopulation waves corresponding to normal (red broken line) and persister cells (blue dashed line). We have used the following parameters for numerical calculations: $\mu_n = 1 \text{ h}^{-1}$, $\mu_p = 0.1 \text{ h}^{-1}$, $D_n = D_p = 100 \mu\text{m}^2 \text{ h}^{-1}$, $a = b = 0.02 \text{ h}^{-1}$. (b) The subpopulation ratio (p/n) at the leading edge and back of the wave follows the theoretically predicted ratios for the exponential growth (dark gray dashed line) and stationary phase (gray dashed line), respectively. (c) Expansion speed (open squares) and persister fraction at the leading edge (closed squares) as functions of the phenotype switching rates (for $a = b$). The solid lines show the corresponding analytical results. (d) The decrease in the expansion speed with the increase in persister fraction at the leading edge (open squares) follows the constitutive relation given by Eq. (4).

Here $n(x, t)$ is the density of a population at position x at time t . To keep the model simple, we consider spatial expansion in one dimension. The two terms on the right-hand side of the equation describe the diffusive spread of the population in space (with a mobility or diffusion coefficient D) and its local logistic growth with growth rate μ . Note that the population size is normalized to the carrying capacity of the logistic growth, i.e., to the maximum population size that can be achieved in the spatially homogeneous conditions. In the following we extend this equation to the case of a population with two distinct phenotypes using bacterial persistence as a concrete example. Bacterial persistence in the presence of antibiotics is associated with an intrinsic phenotypic heterogeneity in the bacterial population. This heterogeneity arises from the stochastic transition between the normal growing cell state and the drug-tolerant persister state at the single-cell level [17]. The two phenotypic states are characterized by different growth (in growth conditions) and death rates (in the presence of antibiotics). To include such phenotype switching into the model, we describe the normal cells and the persister cells by densities $n(x, t)$ and $p(x, t)$, respectively. They are characterized by different growth rates μ_n and μ_p and are subject to a common carrying capacity, such that the constraint on the population size due to the logistic growth acts on the sum $n + p$. In addition, we allow for different

mobility parameters D_n and D_p . A difference in mobility can be expected if movement is due to self-propulsion; if, however, movement is driven by external driving forces, the two parameters will likely be the same. Finally we include phenotype switching: A cell in the normal state can switch to the persister state with a rate a and vice versa with a rate b . These rates are typically small compared to the growth rate [17].

Taking these considerations together, the dynamics of the population composed of normal cells (n) and persister cells (p) can be described by the following coupled differential equations:

$$\begin{aligned} \frac{\partial n}{\partial t} &= D_n \frac{\partial^2 n}{\partial x^2} + \mu_n [1 - (n + p)]n - an + bp, \\ \frac{\partial p}{\partial t} &= D_p \frac{\partial^2 p}{\partial x^2} + \mu_p [1 - (n + p)]p + an - bp. \end{aligned} \quad (2)$$

Like the well-known Fisher equation, these equations display a traveling wave solution. The numerical solution of the above equations is shown in Fig. 1(a) and exhibits a traveling wave for both subpopulations. The numerical solution shows that the fraction of persister cells is small at the leading edge and increases progressively towards the interior of the wave. Far from the leading edge, the subpopulation sizes

are determined by phenotype switching alone and given by $p \approx a/(a+b)$ and $n \approx b/(a+b)$ [in Fig. 1(b), we use equal switching rates ($a=b$), which results in equal subpopulation densities, $n=p=0.5$, in the interior of the wave]. Next, we compute the speed of the population wave as a function of the switching rates. We find that the wave speed decreases with increasing switching rate, while concurrently the persister fraction at the leading edge of the wave increases as shown in Fig. 1(c).

III. RESULTS

A. Characteristic features of the population front

The characteristic features of the population front as presented in Fig. 1 can be understood based on the subpopulation balance during exponential growth and stationary phase in nonmoving conditions. In the absence of movement (diffusion rates are $D_n = D_p = 0$), during the exponential growth phase when the population size is below the carrying capacity (where $n+p \ll 1$), the ratio of persisters to the normal subpopulation is approximately given by $p/n \approx a/(\mu_n - \mu_p)$ [20]. The latter expression follows from a balance of two effects: normal cell outgrow persisters with a rate $\mu_n - \mu_p$, but also regenerate them through switching. In the stationary phase when the population size is near the carrying capacity ($n+p \approx 1$), the ratio of persisters to the normal subpopulation is $p/n \approx a/b$ [20]. In a spatially expanding population (i.e., for finite diffusion rate), the front of the population exhibits the exponential scenario, while the population is in the stationary phase far behind the population front [shown in Fig. 1(b)].

For the classical Fisher wave, the expansion speed is determined by the growth and diffusion via the relation $v = 2\sqrt{D\mu}$. In our case, the growth rate is modulated by the presence of persister cells. This can be demonstrated by deriving an equation for the total population density ($P = n + p$) as

$$\frac{\partial P}{\partial t} = D \frac{\partial^2 P}{\partial x^2} + \mu_{av} P(1 - P), \quad (3)$$

where $\mu_{av} = \mu_n - (\mu_n - \mu_p)f_p$ and $f_p = p/(n+p)$ is the fraction of persisters. Hence, in the presence of phenotype switching, the expansion speed is modulated due to a finite fraction of persisters at the tip of the population wave. We validated this numerically by measuring the wave speed and persister fraction simultaneously at the tip of the wave [as shown in Fig. 1(c)]. The wave speed (denoted by c) and persister fraction (f_p) at the wave front follow the relation [shown in Fig. 1(d)]

$$c = 2\sqrt{D[\mu_n - (\mu_n - \mu_p)f_p]}. \quad (4)$$

For small phenotype switching rates, the subpopulation ratio at the leading edge can be approximated by that for the exponential growth phase, $f_p \approx a/(\mu_n - \mu_p)$, and the wave speed is given by $c \approx 2\sqrt{D(\mu_n - a)}$. In the limit ($a \rightarrow 0$), one recovers the maximal expansion speed (corresponding to a single population without persisters). For our chosen parameters used in Fig. 1, the maximum wave speed is $\approx 20 \mu\text{m h}^{-1}$, which is in the range of measured colony expansion speeds for *Escherichia coli* [26]. Thus, since typically switching rates are small compared to the growth rate, the effect of persisters on

the expansion speed is very small, even if a large subpopulation of persisters exists in the stationary phase situation far from the expansion front.

B. Exact expansion speed

Next, we use standard traveling wave analysis to obtain an analytical expression for the expansion speed over a large range of parameters (for the complete analysis see the Appendix). This method is based on the observation that at long times these traveling waves propagate with constant speed and fixed front shape. This reduces the partial differential equations into an ordinary differential equation with a single variable $z = (x - ct)$, the moving frame of reference. This approach has been used to estimate the expansion speed in reaction-diffusion equations describing population expansion, e.g., in bacterial colony expansion models [3,27–29], in the dynamics of horizontally transmitted traits [30] and cooperative alleles [31] in expanding population waves. Specifically, we use the following ansatz for the subpopulation densities, $n(x, t) = n(x - ct)$ and $p(x, t) = p(x - ct)$ in Eq. (2) and use the resulting equations to determine the stability of the fixed point ($n = 0, p = 0$). The eigenvalues around the fixed point provide a condition for the existence of non-negative and nonoscillatory solutions that determines the minimal value for the wave speed c . Our analysis revealed that traveling waves exist when the following condition (from the requirement that eigenvalues must be real) is satisfied:

$$\frac{c^2}{2D} \geq (\mu_n + \mu_p - a - b) \pm \sqrt{(\mu_n - \mu_p - a + b)^2 + 4ab}. \quad (5)$$

Here the equality provides the minimum wave speed that matches with the numerically computed speed values shown in Fig. 1(c). For equal rates of phenotype switching ($a = b$), the condition for the expansion speed simplifies to $c^2 = 2D(\mu_n + \mu_p - 2a \pm \sqrt{4a^2 + (\mu_n - \mu_p)^2})$. The above condition leads to two distinct values for the expansion speed for which a traveling wave solution exists. We call these the slow and the fast mode, respectively. The slow mode corresponds to a population that contains mostly persister cells, while the fast mode corresponds to a population consisting mostly of normal cells. This can be seen in the limit $a = b = 0$, when the two subpopulation waves decouple with marginal speed $c_{\text{fast}} = \sqrt{2D\mu_n}$ and $c_{\text{slow}} = \sqrt{2D\mu_p}$. In the coupled case (i.e., with finite switching), the expansion speed is given by the faster one of the two moving fronts, i.e., the positive root of the above expression. However, in some cases, the slow mode will also be relevant. An example is a population after crossing an antibiotic zone. Such a population consists almost exclusively of persisters. It will therefore first expand as a slow-mode wave, which will eventually be taken over by a faster wave of normal cells (generated from persister cells that switch to the normal phenotype). This behavior is shown in Fig. 2(a) where the simulation is started with a finite number of persister cells and no normal cells. As the population size increases, the fraction of normal cells increases [shown in Fig. 2(b)], and the whole population advances with the fast mode.

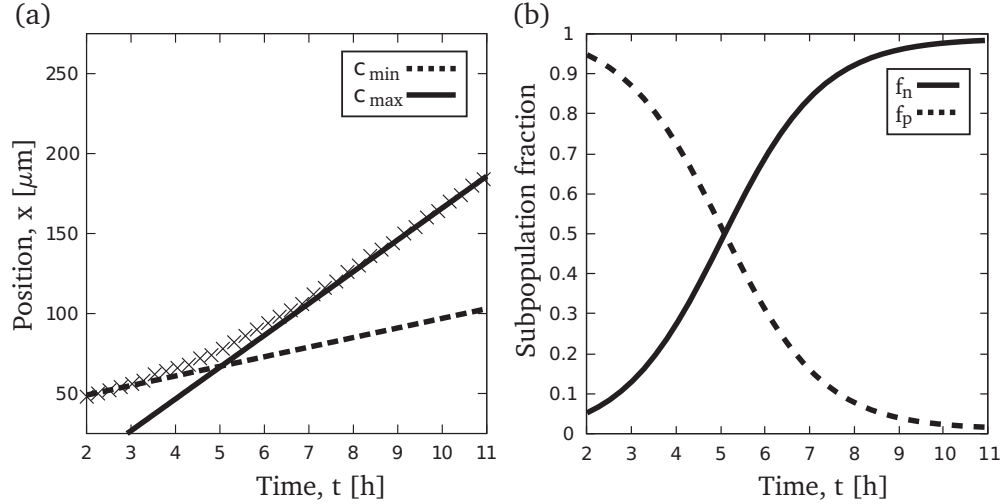


FIG. 2. (a) Expansion speed transitions from a slow (persister-dominated) to a fast (normal cell-dominated) mode as seen in our numerical simulations (cross points) that start with a high persister fraction. The front position as a function of time exhibits the two linear regimes with slopes that match the analytic expressions for the fast (solid line) and slow (broken line) expansion speed. (b) During the speed transition, the fractions of the two phenotypes change; the population shifts from a persister-dominated (broken line) to a normal-cell dominated (solid line) wave.

Comparison of the positive root of the equality in Eq. (5) with Eq. (4) also provides an expression for the persister fraction at the leading edge:

$$f_p = \frac{\mu_n - \mu_p + a + b - \sqrt{(\mu_n - \mu_p - a + b)^2 + 4ab}}{2(\mu_n - \mu_p)}. \quad (6)$$

The expressions for the expansion speed c and the persister fraction f_p show excellent agreement with the respective numerically calculated values [shown in Fig. 1(c)]. The persister fraction f_p reduces to $a/(\mu_n - \mu_p)$ for small switching rates (where $ab \approx 0$) in agreement with the fractions expected in exponential phase for spatially homogeneous populations [20].

C. Extent of penetration of the heterogeneous wave into an antibiotic region

The above results show that spatial expansion results in a small fraction of persisters at the tip of the wave and a larger fraction in the wave interior. This serves as an advantageous trait in the absence of stresses such as antibiotics, as the population expansion is not negatively impacted by persisters, while a persister pool is build up behind the expanding front. If such an expanding population encounters a region that is detrimental to growth, e.g., because of the presence of an antibiotic, the expansion will stall. Population stalling at the interface of an unfavorable environment is known to play a crucial role in the emergence of antibiotic resistance [7], where a key determinant is population survival inside antibiotic environment [32]. Under such stalling conditions, the persister fraction will slowly increase, and cells from the stalled population will enter the unfavorable environment, where the population density decays.

To quantify the effect of bacterial persistence in such scenario, we consider a two-compartment environment containing nutrients permitting growth in one region followed

by a region with bactericidal antibiotics leading to death [7,32,33]. We study the decay of the population density in the antibiotic region [as shown in Fig. 3(a)]. In that region, the population dynamics is described by Eq. (2) with growth terms replaced by death terms (with negative growth rates $-\mu_n^s$ and $-\mu_p^s$ for the normal and persister subpopulation, respectively). We consider the extent to which the wave spreads into the unfavorable environment by calculating the penetration distance x_e into the antibiotic compartment. The extent of the wave is shown for different values of the switching rates in Fig. 3(b). For fixed rate b , the largest extent is seen for the fastest rate of switching from normal to persister state (rate a). Over the full parameter space, the maximum extent occurs for the lowest b and highest a values. Low b values delay the switch back of persisters back to the normal cell state inside the antibiotic region, which contributes effectively to their death rate, and thereby increase the penetration depth. Low values of the switching rate a to the persister state decrease the fraction of persisters at the interface, and thus the penetration depth is increased by high values of a . This situation is analogous to a temporal shift between growth and antibiotic conditions, where faster switching rates to the persister state lead to prolonged survival in the antibiotic conditions. Typically, wild-type strains have low persister fractions with rate $a \ll b$ [19,34] (e.g., $a \approx 10^{-6} h^{-1}$ and $b \approx 10^{-1} h^{-1}$ for *E. coli* wild-type [19]), whereas for high-persistence strains $a \gg b$ (e.g., $a \approx 10^{-3} h^{-1}$ and $b \ll 10^{-4} h^{-1}$ for *E. coli hipQ* mutant [19]). We also note that persister fractions in other bacteria can be much higher than in *E. coli*, implying larger switching rates (e.g., *Staphylococcus aureus* have $a \approx 10^{-3}$ and $b \approx 10^{-1}$ [35]). We find maximum ($\approx 143 \mu\text{m}$) and minimum ($\approx 45 \mu\text{m}$) penetration depth at the opposite ends of the parameter space where the persister fraction is highest ($a = 1$ and $b = 10^{-5}$) and lowest ($a = 10^{-5}$ and $b = 1$), respectively. In general, the penetration depth is determined by the model parameters such as diffusion rates ($D_{n,p}$), death rates ($-\mu_{n,p}^s$),

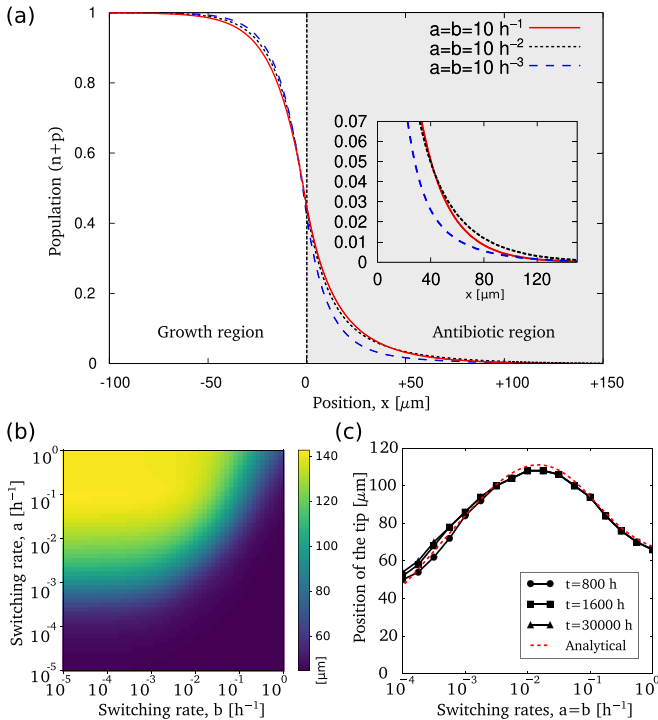


FIG. 3. (a) Steady-state profile of the total population inside an antibiotic region (gray area) for different phenotype switching rates, $a = b = 10^{-1} \text{ h}^{-1}$ (solid red line), 10^{-2} h^{-1} (black broken line), and 10^{-3} h^{-1} (dashed blue line). The inset shows that the population decay is the slowest for an intermediate phenotype switching rate. We have used $\mu_n^s = -1 \text{ h}^{-1}$, $\mu_n^s = -0.1 \text{ h}^{-1}$ and other parameters are the same as in Fig. 1. (b) The penetration depth of the population wave into the antibiotic region as a function of the switching rates a and b . It is computed as the distance of the position where $n(x_e) + p(x_e) = N_{\text{tip}}$ ($N_{\text{tip}} = 0.005$ in the simulations). (c) For equal rates $a = b$, the plot shows the existence of a phenotype switching rate, for which the extent of the wave into the antibiotic region is maximal.

population density detection limit (N_{tip}), etc., that depends on the experimental conditions. When all the parameters except switching rates are similar between different strains, our analysis predicts that a high persistence strain will show a larger penetration depth than a wild-type strain. Interestingly, using a tolerance detection test, Gefen *et al.* [33] recently demonstrated that, in a gradient of antibiotic concentration, a high persistence strain is found deeper into the high antibiotic concentration region than the wild-type strain as detected after replenishing with nutrients. This situation differs from our case in two respects: it is based on a smooth gradient of antibiotic rather than a sharp threshold and an already established population grows and reacts to the addition of an antibiotic addition in a certain region. Nevertheless, our simulations show that the steady-state population density profile would be identical for both types of dynamics, i.e., for a spatially expanding population and for space-dependent selection in a previously established population (Fig. 8 below).

In the specific scenario, where the two rates are varied together ($a = b$), the penetration depth of the wave displays a maximum for intermediate phenotype switching rates

[Fig. 3(c)], which reflects the two opposing requirements on the two rates. The cost associated with switching back to normal cells (increased death rate in the antibiotic region) is balanced by increased survival due to a larger persister subpopulation entering the antibiotic region only for intermediate switching rates. These considerations can be made more precise by analyzing the steady-state density profile in the antibiotic region (discussed in the Appendix). The red dashed line in Fig. 3(c) shows that the population extent estimated from steady-state density profile agrees well with the corresponding numerical results.

The extended distance over which the population decays within the antibiotic region due to the presence of persisters can also support the crossing of such a region of finite width, i.e., an antibiotic barrier, a scenario we have previously studied in a model with discrete spatial compartments [21]. We found that the presence of persister cells can decrease the mean first arrival time of cells in a growth environment behind an antibiotic barrier. The same is seen in the continuous-space model described by the two-subpopulation Fisher equation that we study here. Specifically, we find a minimum in the crossing time as the switching rates are varied (discussed in the Appendix).

D. Population expansion in spatially varying environments containing growth and antibiotic regions

The above results suggest that the presence of persisters provides a benefit when a population has to cross an antibiotic environment and thus, likely for expansion in spatially heterogeneous environments that contain antibiotic regions. Previous theoretical studies [18,19], including ours [20,21], have shown the existence of optimal switching rates in temporally varying environments that are tuned to the environment duration. To investigate if a similar behavior exists in spatially periodic environments, we next study population expansion in environments that alternate between growth sustaining conditions and antibiotic conditions.

First, we focus on expansion in environments with identical widths for the growth and antibiotic regions. For small widths of the two regions, we did not observe any maximum in the expansion speed; rather, the maximal speed is in the limiting case without persisters [Fig. 4(a)]. In this case, for fixed values of switching rate b (from the persister state back to normal state), an increase in persister formation rate (a) decreases the expansion speed. This trend is in contrast to the case for the extent of the wave in the antibiotic region. This is due to a large fraction of persister (for high a values) in the antibiotic region that delays fast expansion in the subsequent growth region [as discussed in Fig. 2(a)].

For larger widths of both regions, we find a global maximum in the expansion speed in a, b space as shown in Fig. 4(b). The transitions between the two regimes, i.e., with and without speed maximum, depend on the width of the environments Fig. 4(a). For our parameter values, this transition occurs for spatial period, $X \gtrsim 100 \mu\text{m}$. Further, the optimal switching rates decrease with an increase in the environmental period. This behavior is analogous to temporally varying periodic environments, but with one difference: the optimal switching rates are unequal even for equal widths of the two

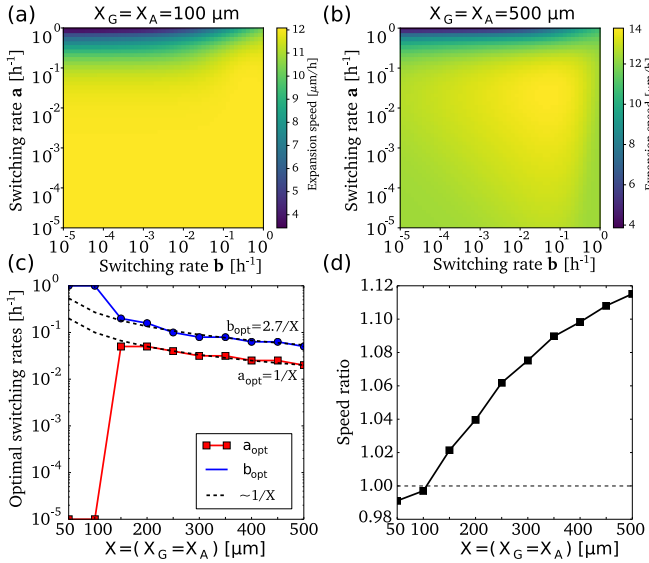


FIG. 4. Expansion in symmetric periodic environments. (a) Expansion speed of the population for different switching rates (a , b) for a short environmental width ($X_G = X_S = X = 50 \mu\text{m}$). The expansion speed decreases with the increase in b for fixed a values. The maximum value of the expansion rate lies in the region with the lowest switching rates. (b) Same as in (a) for a long environmental width ($X_G = X_S = X = 100 \mu\text{m}$). (c) The switching rates (a_{opt} , b_{opt}) corresponding to the maximal expansion speed (obtained from maps like in b) varies inversely with the environmental widths (X). (d) The ratio between the maximum expansion speed in the presence of persistence and the speed without persistence for different environmental widths. The benefit (where the ratio is > 1) from persistence exists only after a threshold value for the environment's width. Note that the plotted values are based on the maximal expansion speed observed in the simulated parameter range. Values < 1 indicate that the limiting case without persisters (not included in the simulated parameter range) gives the maximal expansion speed.

environments. The optimal rate b is found to be about three times higher than the optimal rate a . This difference could come from the fact that in the case of temporal variation, the two environmental conditions are coupled through initial conditions only, whereas for spatial variation, the two environments are coupled by diffusive flux at the interfaces. The benefit due to the presence of persistence is shown in Fig. 4(d) by computing the ratio of expansion speed with the optimal switching rates and in the absence of phenotype switching. Notably, the transition between the regimes where absence of persisters is optimal and the regime with finite optimal switching rates can be identified here by considering where the speed ratio crosses from values < 1 , i.e., no benefit of switching, to values > 1 corresponding to a benefit of phenotype switching.

Next we consider the case of a fixed width of the growth region ($X_G = 400, 200 \mu\text{m}$) and vary the width of the antibiotic region ($X_A \leq X_G$), as shown in Figs. 5(a) and 5(b). For a fixed growth region width, an increase in the width of the antibiotic region leads to a transition from no switching to a finite switching rate as the optimal strategy for maximal expansion speed. Our results in Fig. 5(a) for $X_G = 200 \mu\text{m}$ (dashed line points) and $X_G = 400 \mu\text{m}$ (solid line points) show that the optimal switching rate b_{opt} decreases inversely

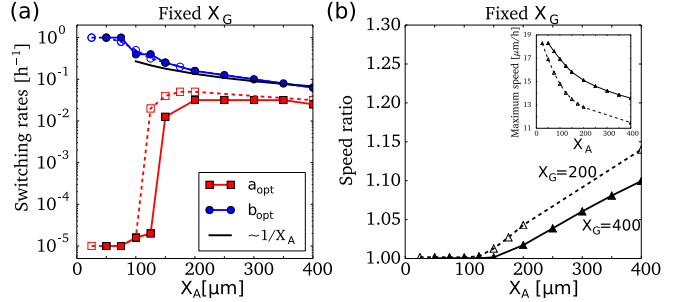


FIG. 5. Expansion in asymmetric periodic environments. (a) Optimal switching rates (a_{opt} shown by squares, b_{opt} shown by circles) as a function of the antibiotic region width for a fixed growth region width ($X_G = 400 \mu\text{m}$ and $X_G = 200 \mu\text{m}$ in solid and broken lines, respectively) (b) Ratio of expansion speed with optimal switching rates and without any phenotype switching for different antibiotic region widths. The inset shows the absolute value of the maximum speed for $X_A = 200 \mu\text{m}$ and $X_A = 400 \mu\text{m}$.

with the width of antibiotic region X_A , whereas the switching rate a_{opt} remains almost constant. A similar sharp transition from no switching to a finite switching rate is also observed in temporally periodic environments when the duration of antibiotic exposure is increased [28]. Further, with the emergence of (finite-rate) switching as an optimal strategy, the fold change in expansion rate increases above 1 as shown in Fig. 5(b). Interestingly the advantage of phenotype switching through the increased expansion speed is higher for the shorter growth region.

IV. DISCUSSION

Theoretical and experimental studies have shown stochastic switching between distinct phenotypes in bacterial population as a bet-hedging strategy for temporally varying environments [18–20,36–39]. A recent study showed bet hedging is more favorable in spatially varying environments compared to temporally varying environments [40]. However, it is unclear how stochastic switching dictates bacterial growth in spatially varying environment. Here we have used a Fisher wave approach to investigate the spatial expansion of a bacterial population with stochastic phenotype switching for three scenarios, a spatially homogeneous environment, an interface between a growth environment and an antibiotic region and a spatially periodic environment. The cost of the presence of persisters during growth-favorable conditions is quantified by the population expansion speed, for which we obtained analytical expression. For typical switching rates, this cost is very small, even if there is a substantial persister fraction in behind the wave front, because the tip of the population wave contains a rather small fraction of persister cells. The persister pool in the back of the wave acts as a reservoir for the case of encountering stressful environments. The subpopulation redistribution from the tip to the back of the wave occurs at a slower rate than the population expansion (discussed in the Appendix). This contributes to the low cost associated with persistence. At an boundary to a stress environment such as an antibiotic barrier, the sub-population structure has to catch up with the wave tip, which results in transient stalling of

the expansion. Eventually, the number of persister cells at the boundary increases due to subpopulation redistribution, helping the population wave to spread into the antibiotic region, thus providing the fitness advantage conferred by the presence of persisters. Further, we found optimal switching rates for spatially varying environments reminiscent of optimal switching rates for growth in temporally varying environments [18–20]. In summary, our study reveals an added advantage of bacterial persistence in spatial environments which may play an important role in bacterial invasion and in the development of antibiotic resistance, where persisters may provide a pool from which resistance can emerge.

APPENDIX

1. Phenotypic redistribution in interior of the expanding wave

To quantify the change in phenotypic redistribution from the leading edge to the interior of the wave, we define a phenotypic flux as $J = (\frac{a}{a+b} n - \frac{b}{a+b} p)$. The phenotypic flux balances out in the interior of the wave, i.e., $J = 0$. In the moving frame of reference ($z = x - ct$), the phenotypic flux increases (and persister fraction decreases) from zero at the interior of the wave to the front of the wave. The increase in J inside the fully populated region (with $n + p = 1$ and $D = D_n = D_p$) is governed by a diffusion-decay equation,

$$\frac{\partial J}{\partial t} = D \frac{\partial^2 J}{\partial x^2} - (a + b)J. \quad (\text{A1})$$

For an expanding population, the phenotypic flux in the moving frame of reference thus increases as

$$J = J_0 \exp \left[z \left(\sqrt{c^2 + 4D(a+b)} - c \right) \right] \\ \approx J_0 \exp \left[(x - ct) \sqrt{\frac{D}{\mu_n} \left(\frac{a+b}{2} \right)} \right]. \quad (\text{A2})$$

The above expression shows that subpopulation redistribution occurs at a slower rate [with rate constant $\approx \sqrt{\frac{D}{\mu_n} \left(\frac{a+b}{2} \right)}$ for small ab] and that the subpopulation redistribution process lags behind the advancing wave as shown in Fig. 6. Therefore for small switching rates, spatial expansion results in keeping fraction of persisters at the tip of the wave small despite a large fraction of persisters in the interior of the wave.

2. Wave speed determination through traveling wave analysis

Using the wave solution ansatz

$$n(x, t) = n(x - ct), \quad p(x, t) = p(x - ct) \quad (\text{A3})$$

and introducing auxiliary variables $n' = dn/dz$ and $p' = dp/dz$ with $z = x - ct$, Equations (2) can be expressed as the following set of autonomous first-order differential equations:

$$\frac{dn}{dz} = n', \quad \frac{dp}{dz} = p', \\ \frac{dn'}{dz} = -\frac{c}{D_n} n' - \frac{\mu_n}{D_n} (1 - P)n + an - bp, \\ \frac{dp'}{dz} = -\frac{c}{D_p} p' - \frac{\mu_p}{D_p} (1 - P)p - an + bp, \quad (\text{A4})$$

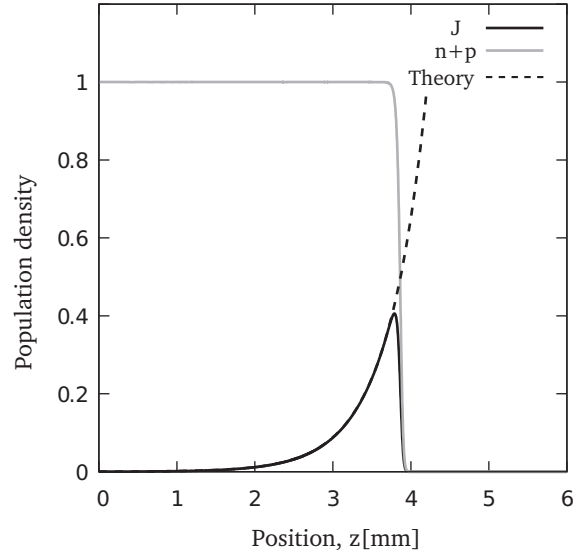


FIG. 6. Phenotypic flux distribution along the wave in the moving frame of reference (z). In the populated regions (where $n + p = 1$), the phenotypic flux J (solid black line) increases exponentially from the back of the wave to the front, in excellent agreement with the analytical expression for J (dashed black line).

which can be analyzed by the standard fixed point analysis for traveling wave solutions. The eigenvalues (λ) of the above equations near the fixed point $n' = 0$, $p' = 0$, $n = 0$, $p = 0$ is given by the following fourth-order equation:

$$D_n D_p \lambda^4 + c(D_n + D_p) \lambda^3 + (c^2 + D_n(\mu_p - b) \\ + D_p(\mu_n - a)) \lambda^2 + c(\mu_n + \mu_p - a - b) \lambda \\ + (\mu_n \mu_p - \mu_n b - \mu_p a) = 0.$$

For simplicity, we take $D_n = D_p = D$. The four roots ($\lambda_{1,2,3,4}$) are then given by

$$\lambda_{1,2,3,4} = -\frac{c \pm \sqrt{c^2 - 2D(\mu_n + \mu_p - a - b \pm \sqrt{\Delta})}}{2D}$$

with $\Delta = (a + b)^2 + (\mu_n - \mu_p)^2 - 2(\mu_n - \mu_p)(a - b)$. For the existence of a stable traveling wave solution, these eigenvalues must be real. This leads to the condition

$$c^2 \geq 2D(\mu_n + \mu_p - a - b \pm \sqrt{\Delta}), \quad (\text{A5})$$

which for $a = b$ simplifies to

$$c^2 \geq 2D \left(\mu_n + \mu_p - 2a \pm \sqrt{4a^2 + (\mu_n - \mu_p)^2} \right). \quad (\text{A6})$$

In the limit $a = b = 0$, the two conditions result in the marginal speeds of two uncoupled waves, $c_{\text{fast}} = \sqrt{2D\mu_n}$ and $c_{\text{slow}} = \sqrt{2D\mu_p}$. In the coupled case, the wave speed is given by the faster moving wave, i.e., the positive root.

3. Population decay in the antibiotic region

In the absence of phenotype switching, the normal population decays exponentially [as $n(x) = n_0 \exp(-x\sqrt{\mu_n^2/D})$] in the antibiotic region, and the penetration depth is given by $x_e = \sqrt{D/\mu_n^2} \ln(n_0/N_{\text{tip}})$. For finite phenotype switching, the

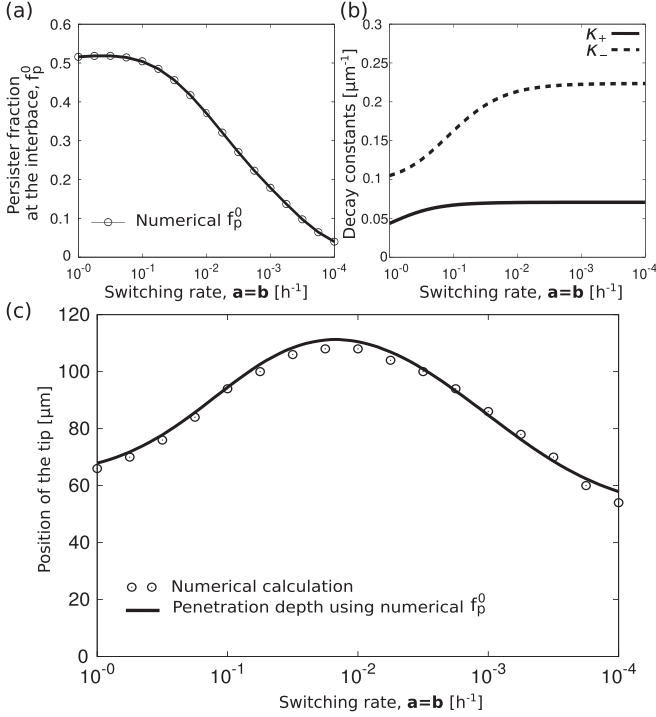


FIG. 7. (a) Persister fraction at the boundary of growth and antibiotic regions as a function of the phenotype switching rate ($a = b$, open circles). For large switching rate, the persister fraction approaches $f_{p,\max} = 0.5$ due to equal switching rates. (b) Two characteristic decay constants of the population density in the antibiotic region, κ_+ (solid line) and κ_- (dashed line). Both are decreasing functions of the switching rate. (c) The impact of the switching rate on the persister fraction at the boundary and on κ_- is sufficient to explain the maximum in the extent of the wave as a function of the phenotype switching rate (open circles are from the numerical calculation). The solid line uses Eq. (A9) together with the numerical values of f_p^0 .

population dynamics in the antibiotic region at the steady state is given by the following coupled diffusion-decay equations:

$$\begin{aligned} 0 &= D \frac{d^2 n}{dx^2} - \mu_n^s n - an + bp, \\ 0 &= D \frac{d^2 p}{dx^2} - \mu_p^s p + an - bp. \end{aligned} \quad (\text{A7})$$

These equation can be solved for boundary conditions $n(x_b, 0) = n_0$ and $p(x_b, 0) = p_0$, from which we obtain the following subpopulation profile (for $a = b$, $D_n = D_p = D$):

$$\begin{aligned} n(x) &= \frac{1}{(l_+ - l_-)} \\ &\quad \times [(2ap_0 - l_- n_0)e^{-x/\kappa_-} + (l_+ n_0 - 2ap_0)e^{-x/\kappa_+}], \\ p(x) &= \frac{1}{(l_+ - l_-)} \\ &\quad \times [(2an_0 + l_+ p_0)e^{-x/\kappa_-} - (l_- p_0 + 2an_0)e^{-x/\kappa_+}] \end{aligned}$$

with $l_{\pm} = D^{-1}[(\mu_n - \mu_p) \pm \sqrt{4a^2 + (\mu_n - \mu_p)^2}]$ and $\kappa_{\pm} = \sqrt{2D[(2a + \mu_n + \mu_p) \pm \sqrt{4a^2 + (\mu_n - \mu_p)^2}]^{-1}}$.

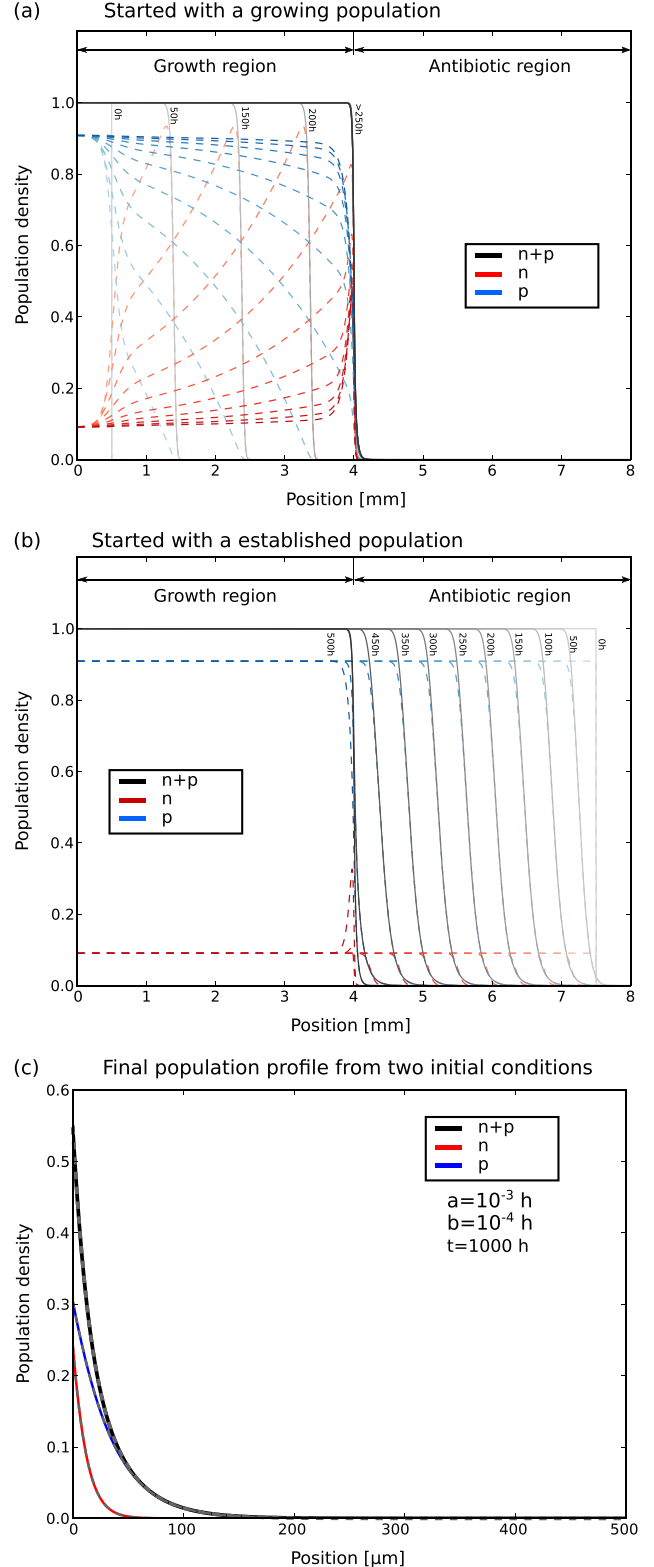


FIG. 8. (a) Expanding population stalled by an antibiotic region. Initial conditions: $n + p = 1$ with $n/p = b/a$ for $x < 5$ mm, otherwise 0. (b) Established population decaying due to the addition of the antibiotic region. Initial conditions: $n + p = 1$ with $n/p = b/a$ for $x < 75$ mm, otherwise 0. (c) Population density profile for the case (a) and case (b) overlap each other, indicating that steady state is independent of initial condition. The switching rates are $a = 10^{-3} h$ and $a = 10^{-4} h$.

The above analytical solution shows that the subpopulation decays exponentially with two characteristic decay constants κ_{\pm} . The slow decay term with decay constant κ_{-} dominates far into the antibiotic region, where the total population profile can be approximated as

$$n + p \approx \frac{[2a(n_0 + p_0) + l_+ p_0 - l_- n_0]}{(l_+ - l_-)} e^{-\frac{x}{\kappa_-}}. \quad (\text{A8})$$

From this expression of the profile, we obtain the penetration depth as

$$x_e = \kappa_-(a) \ln \left(\frac{(n_0 + p_0)\phi(f_p^0)}{N_{\text{tip}}} \right), \quad (\text{A9})$$

where $\kappa_- = \sqrt{2D[(\mu_n^s + \mu_p^s + 2a) - \sqrt{4a^2 + (\mu_n^s - \mu_p^s)^2}]^{-1}}$ and

$$\phi(f_p(a)) = \frac{a + (\mu_n^s - \mu_p^s)f_p^0(a) - l_-/2}{\sqrt{4a^2 + (\mu_n^s - \mu_p^s)^2}} \quad (\text{A10})$$

is a function of the parameters of the dynamics and of the persister fraction at the compartment boundary, $f_p^0(a)$. Therefore, the decay of the population wave in the antibiotic region is governed by two factors: the spatial decay constant $\kappa_-(a)$ and a function of persister fraction $f_p^0(a)$ at the interface between growth and antibiotic, both of which are a function of phenotype switching rate. The decay constant κ_- is a decreasing function in a [as shown in Fig. 7(b)] whereas $f_p^0(a)$ is an increasing function [as shown in Fig. 7(a)]. The combination of these two opposing behaviors explains the nontrivial maximum in the extent of the wave with the variation in phenotype switching rates. In Fig. 7(c) we compare the analytical expression of the extent of the wave to the numerically computed value. Further we show that the extent of the wave is independent of the initial conditions (Fig. 8).

4. Crossing of an antibiotic barrier

To study crossing of an antibiotic region, we numerically calculate the crossing time of an expanding population facing a spatially extended antibiotic barrier of finite width (the schematic is depicted in Fig. 9 inset; we determine the crossing time as the time between the arrival of the tip of the wave at the first and second interface). We find the crossing

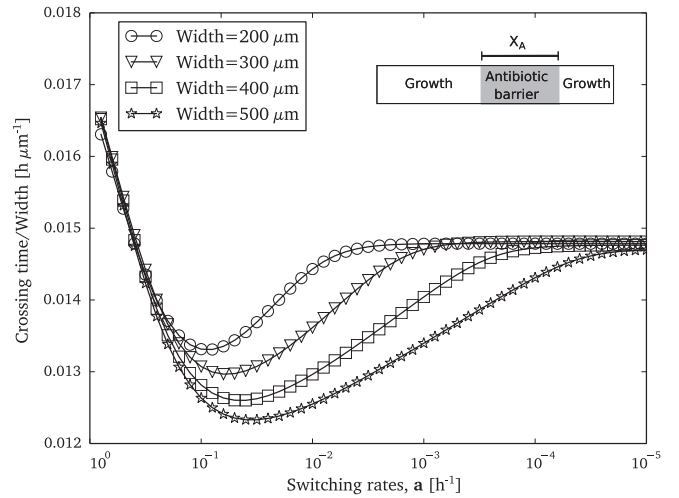


FIG. 9. Antibiotic barrier crossing time of the population as a function of the phenotype switching rate a for different barrier widths. The crossing time is normalised with respect to the barrier width. The inset schematic depicts the simulation setup. A long growth region is chosen to allow the population to reach a steady state (for each a value) before facing the antibiotic barrier.

time to show a nonmonotonic behavior as a function of the increase in the phenotype switching rate, as shown in Fig. 9. Specifically, we observe a minimum at intermediate switching rates that reflects the maximum of the penetration depth into the antibiotic region discussed above. At very low switching rates, as one would expect for a population with no persisters, the crossing time scales with the width of the barrier, and their ratio becomes independent of the width and approaches similar values as shown in Fig. 9. Similarly for very fast switching rates, the persister population first crosses the barrier, and hence the crossing time again scales with barrier width. For intermediate switching rates, the ratio of crossing time and barrier width depends both on the rate of phenotype switching and the width. This is because both normal and persister subpopulation contribute to barrier crossing but at different length scales; the normal cells dominate crossing over narrow barriers, while the persister cells enable crossing of wider barriers.

[1] G. M. Hewitt, *Biol. J. Linn. Soc.* **58**, 247 (1996).
 [2] D. Tilman and P. M. Kareiva, *Spatial Ecology: The Role of Space in Population Dynamics and Interspecific Interactions* (Princeton University Press, Princeton, 1997).
 [3] K. S. Korolev, M. J. I. Müller, N. Karahan, A. W. Murray, O. Hallatschek, and D. R. Nelson, *Phys. Biol.* **9**, 026008 (2012).
 [4] T. Reichenbach, M. Mobilia, and E. Frey, *Nature (London)* **448**, 1046 (2007).
 [5] M. S. Datta, K. S. Korolev, I. Cvijovic, C. Dudley, and J. Gore, *Proc. Natl. Acad. Sci. USA* **110**, 7354 (2013).
 [6] O. Hallatschek, P. Hersen, S. Ramanathan, and D. R. Nelson, *Proc. Natl. Acad. Sci. USA* **104**, 19926 (2008).

[7] M. Baym, T. D. Lieberman, E. D. Kelsic, R. Chait, R. Gross, I. Yelin, and R. Kishony, *Science* **353**, 1147 (2016).
 [8] Q. Zhang, G. Lambert, D. Liao, H. Kim, K. Robin, C.-K. Tung, N. Pourmand, and R. H. Austin, *Science* **333**, 1764 (2011).
 [9] J. E. Keymer, P. Galajda, G. Lambert, D. Liao, and R. H. Austin, *Proc. Natl. Acad. Sci. USA* **105**, 20269 (2008).
 [10] M. Hegreness, N. Shores, D. Damian, D. Hartl, and R. Kishony, *Proc. Natl. Acad. Sci. USA* **105**, 13977 (2008).
 [11] J. Molofsky, J. D. Bever, and J. Antonovics, *Proc. R. Soc. Lond. B* **268**, 273 (2001).
 [12] R. Hermsen and T. Hwa, *Phys. Rev. Lett.* **105**, 248104 (2010).

- [13] N. Dhar and J. D. McKinney, *Curr. Opin. Microbiol.* **10**, 30 (2007).
- [14] K. Lewis, *Nat. Rev. Microbiol.* **5**, 48 (2007).
- [15] J. Bigger, *Lancet* **244**, 497 (1944).
- [16] G. R. Stewart, B. D. Robertson, and D. B. Young, *Nat. Rev. Microbiol.* **1**, 97 (2003).
- [17] N. Q. Balaban, J. Merrin, R. Chait, L. Kowalik, and S. Leibler, *Science* **305**, 1622 (2004).
- [18] E. Jablonka, B. Oborny, I. Molnár, E. Kisdi, J. Hofbauer, and T. Czárán, *Philos. Trans. R. Soc. Lond. B* **350**, 133 (1995).
- [19] E. Kussell, R. Kishony, N. Q. Balaban, and S. Leibler, *Genetics* **169**, 1807 (2005).
- [20] P. Patra and S. Klumpp, *PLoS ONE* **8**, e62814 (2013).
- [21] P. Patra and S. Klumpp, *Phys. Rev. E* **89**, 030702(R) (2014).
- [22] R. A. Fisher, *Ann. Eugen.* **7**, 355 (1937).
- [23] J. G. Skellam, *Biometrika* **38**, 196 (1951).
- [24] A. N. Kolmogorov, I. G. Petrovsky, and N. S. Piskunov, *Bulletin of Moscow State University Series A: Mathematics and Mechanics* **1**, 1 (1937).
- [25] G. Lambert, D. Liao, S. Vyawahare, and R. H. Austin, *J. Bacteriol.* **193**, 1878 (2011).
- [26] M. R. Warren, H. Sun, Y. Yan, J. Cremer, B. Li, and T. Hwa, *eLife* **8**, e41093 (2019).
- [27] F. D. C. Farrell, O. Hallatschek, D. Marenduzzo, and B. Waclaw, *Phys. Rev. Lett.* **111**, 168101 (2013).
- [28] P. Patra, K. Kissoon, I. Cornejo, H. B. Kaplan, and O. A. Igoshin, *PLoS Comput. Biol.* **12**, e1005010 (2016).
- [29] F. Beroz, J. Yan, Y. Meir, B. Sabass, H. A. Stone, B. L. Bassler, and N. S. Wingreen, *Nat. Phys.* **14**, 954 (2018).
- [30] J. Venegas-Ortiz, R. J. Allen, and M. R. Evans, *Genetics* **196**, 497 (2014).
- [31] K. S. Korolev, *PLoS Comput. Biol.* **9**, e1002994 (2013).
- [32] F. J. Hol, B. Hubert, C. Dekker, and J. E. Keymer, *ISME J.* **10**, 30 (2016).
- [33] O. Gefen, B. Chekol, J. Strahilevitz, and N. Q. Balaban, *Sci. Rep.* **7**, 41284 (2017).
- [34] B. Van den Bergh, J. E. Michiels, T. Wenseleers, E. M. Windels, P. V. Boer, D. Kestemont, L. De Meester, K. J. Verstrepen, N. Verstraeten, M. Fauvart *et al.*, *Nat. Microbiol.* **1**, 16020 (2016).
- [35] S. Lechner, P. Patra, S. Klumpp, and R. Bertram, *J. Mol. Microbiol. Biotechnol.* **22**, 381 (2012).
- [36] M. Thattai and A. van Oudenaarden, *Genetics* **167**, 523 (2004).
- [37] B. Gaál, J. W. Pitchford, and A. J. Wood, *Genetics* **184**, 1113 (2010).
- [38] E. Kussell and S. Leibler, *Science* **309**, 2075 (2005).
- [39] M. Lachmann and E. Jablonka, *J. Theor. Biol.* **181**, 1 (1996).
- [40] P. V. Martín, M. A. Muñoz, and S. Pigolotti, *PLoS Comput. Biol.* **15**, e1006529 (2019).